


Original Paper

# Non-stationary Geostatistical Modeling: A Case Study Comparing LVA Estimation Frameworks

Ryan Martin <sup>1,3</sup> David Machuca-Mory,<sup>2</sup> Oy Leuangthong,<sup>2</sup> and Jeff B. Boisvert<sup>1</sup>

Received 10 March 2018; accepted 20 May 2018

Published online: 29 May 2018

Incorporating locally varying anisotropy (LVA) in geostatistical modeling improves estimates for structurally complex domains where a single set of anisotropic parameters modeled globally do not account for all geological features. In this work, the properties of two LVA-geostatistical modeling frameworks are explored through application to a complexly folded gold deposit in Ghana. The inference of necessary parameters is a significant requirement of geostatistical modeling with LVA; this work focuses on the case where LVA orientations, derived from expert geological interpretation, are used to improve the grade estimates. The different methodologies for inferring the required parameters in this context are explored. The results of considering different estimation frameworks and alternate methods of parameterization are evaluated with a cross-validation study, as well as visual inspection of grade continuity along select cross sections. Results show that stationary methodologies are outperformed by all LVA techniques, even when the LVA framework has minimal guidance on parameterization. Findings also show that additional improvements are gained by considering parameter inference where the LVA orientations and point data are used to infer the local range of anisotropy. Considering LVA for geostatistical modeling of the deposit considered in this work results in better reproduction of curvilinear geological features.

**KEY WORDS:** Kriging, Local anisotropy, Non-stationarity.

## INTRODUCTION

Anisotropy describes differing continuity of a regionalized variable (RV) depending on orientation in a domain (Rossi and Deutsch 2014). Geostatistical modeling with anisotropy is required for geological variables deposited preferentially along specific orientations related to different geological processes and structural orientations. Modeling

global anisotropy requires calculation of the experimental variogram along three mutually perpendicular orientations chosen based on geological properties and/or grade continuity. Experimental variogram points are fit with an appropriate variogram model, and the resulting range to the sill defines the magnitude of continuity along each direction. Anisotropy is fully parameterized by a set of three rotation angles (strike, dip and plunge), and two magnitude ratios  $r_1 = \frac{a_2}{a_1}$  and  $r_2 = \frac{a_3}{a_1}$ , where  $a_1$ ,  $a_2$  and  $a_3$  are the ranges along each principal axis, and generally  $a_1 \geq a_2 \geq a_3$ ; the rotation angle conventions from Rossi and Deutsch (2014) are used here. However, for domains with complex spatial patterns, a single global set of anisotropic parameters do not

<sup>1</sup>Center for Computational Geostatistics, University of Alberta, Edmonton, Canada.

<sup>2</sup>SRK Consulting (Canada) Inc., 155 University Ave., Suite 1500, Toronto, ON, Canada.

<sup>3</sup>To whom correspondence should be addressed; e-mail: rdm1@ualberta.ca

satisfy the local properties of the data. To address this issue, frameworks for modeling with locally varying anisotropy (LVA) have been developed (Xu 1996; te Stroet and Snepvangers 2005; Sullivan et al. 2007; Boisvert and Deutsch 2011; Machuca-Mory and Deutsch 2013; Fouedjio 2016).

Methods to model LVA and generate geostatistical models with LVA depend on site-specific characteristics and the tools and data available to parameterize each modeling algorithm. Techniques for geostatistical modeling with LVA include: manual or automated domain partitioning (Martin and Boisvert 2017); stratigraphic transformations; unfolding; locally weighted statistics (Machuca-Mory and Deutsch 2013; Fouedjio et al. 2016); or space deforming algorithms (Boisvert and Deutsch 2011; Fouedjio et al. 2015). From the view of the practitioner, the technique to implement depends on the complexity of the structural features and the nature of the information available to parameterize each framework. Generally, the simplest method that can account for the features of interest should be implemented; however, the information available to parameterize the LVA may restrict which algorithms can be applied. Simple to moderately complex structural relationships may be captured with manual or automated domain partitioning, stratigraphic transformations or unfolding; generally, these methods require fewer input parameters. For example, a stratigraphic transformation is suitable for simpler geometries where a reference datum can be identified across different areas. Similarly, a manual partitioning workflow requires knowledge of the grade continuities in different zones to justify subsetting the deposit. More complex structural features can be accounted for by assuming local stationary and overlapping windows, but this requires the inference of local statistics with, for example, the distance-weighted statistics from Machuca-Mory and Deutsch (2013). The shortest-paths-based LVA method from Boisvert and Deutsch (2011) is the most complex method to incorporate LVA to geostatistical modeling but can capture nonlinear features at a scale finer than the data spacing. For more complex LVA modeling techniques, the use of information external to the point data (e.g., secondary data, geological models) can enhance the LVA model by providing local continuity information not explicitly captured in the point data.

Grades estimated with LVA better reproduce locally oriented features in structurally complex

domains, mainly determined by visually inspecting grade models in different areas. Past works have also shown that modeling with LVA can improve cross-validation results (Boisvert and Deutsch 2011; Machuca-Mory and Deutsch 2013; Fouedjio 2015; Fouedjio and Seguret 2016). Thus, for domains with complex spatial patterns, there is clear motivation for adopting an LVA framework for estimation. However, the choice of LVA framework and differences in parameter inference can lead to large and potentially subjective differences between resource models.

This work studies two classes of geostatistical modeling with LVA applied to a case study dataset. The first class makes a Markov assumption and uses local variogram parameters to estimate the conditional distribution at the unsampled locations. The second class uses space deformation where the input space is deformed such that spatial continuity in the deformed space is described by a stationary isotropic covariance function. The parameterization of the LVA represents a major consideration for any geostatistical modeling with LVA. In this work, a geological boundary model defines the directions of local continuity, but associated ranges of anisotropy are required to completely parameterize the LVA. Four methodologies are considered to infer these local ranges, including: manual interpretation, cross-validation and methods that utilize the local orientations and point data to calculate the local range of anisotropy.

This paper is organized as follows: First, the different frameworks for generating geostatistical models with LVA are summarized. Next, methods to infer the required parameters for each framework are explored. Finally, the effects of different LVA-estimation frameworks and LVA-field parameterizations are examined by visual inspection and with cross-validation on the case study dataset.

## SECOND-ORDER NON-STATIONARY TECHNIQUES AND PARAMETERIZATION

Geostatistical modeling with a spatially varying covariance function has been studied extensively (Xu 1996; te Stroet and Snepvangers 2005; Sullivan et al. 2007; Boisvert and Deutsch 2011; Machuca-Mory and Deutsch 2013; Fouedjio 2016). A summary of the different methods is given here, but for a comprehensive review the reader is directed to

Fouedjio (2016). Of all the methods, there are generally two groups: location-dependent kriging parameters and space deformations.

The first group of non-stationary estimation depends on a location-dependent set of variogram and statistical parameters. In this class of non-stationary estimation, a Markov assumption is made and the kriging neighborhood is restricted to the  $N$  nearest neighbors found in a local search (Xu 1996; Machuca-Mory and Deutsch 2013). Under this assumption, the parameters informing the local kriging system of equations can be unique for all locations in the domain and resulting estimates reflect these local anisotropic properties. Xu (1996) demonstrates the utility of this method for a sparse environment by showing that conditional simulations better reproduced nonlinear geological patterns when considering LVA.

The second group of non-stationary estimation implements a space deformation where the non-stationary features of the RV in Cartesian space are embedded in a new space where the spatial continuity is described by a stationary isotropic covariance function (Boisvert and Deutsch 2011; McBratney and Minasny 2013; Fouedjio 2015). Various techniques are used to accomplish the embedding or space deformations; the shortest-path and nonlinear-distance framework from Boisvert and Deutsch (2011) is considered here. Although space deformations can be used to capture features present at a scale finer than the data spacing, this implies an external source of information for parameter inference since these features cannot be inferred solely from the point data used in estimation.

Parameterizing the local features for each framework represents the fundamental workflow for implementing different second-order non-stationary estimation methods. Xu (1996) proposed to conditionally simulate local orientations for sparse-data environments where the measurements of local orientation are available at a few locations. Alternatively, te Stroet and Snepvangers (2005) propose an iterative algorithm where local orientations are gradually refined from previous estimated models, mainly targeting densely sampled domains. The distance-weighted local variogram (DWLV) approach (Machuca-Mory and Deutsch 2013; Fouedjio et al. 2016) provides a comprehensive framework for calculating all local parameters from the input dataset. At a set of anchor locations, defined at a resolution coarser than the data locations, the mean,

variance and variogram are inferred using a distance-based weighting scheme that ensures nearby data have the most influence at each anchor location. These locally inferred parameters are then interpolated from the anchor locations to all estimation locations to inform the local kriging parameters. The method from Fouedjio et al. (2016) is similar to the DWLV method but mainly developed for 2D domains. For complex 3D domains, Machuca-Mory and Deutsch (2013) note that extra information is required to inform the orientations for local variogram calculations. Notably, LVA parameters inferred from the data may only capture variability at a scale equal to or larger than the data scale.

The ideal source of information for LVA techniques is an external source that adds information to the model, e.g., geological interpretations, related soft secondary data, etc. For complex and/or sparsely sampled domains, the inclusion of local orientations from an external source adds information that cannot be derived from local statistics or bootstrapping previous models. In fact, the added information can also benefit densely sampled domains where the target variable is discontinuous at a short range, as is the case in structurally hosted gold deposits. Lillah and Boisvert (2015) develop several methods to extract local orientations from a variety of external data sources. Local orientations may also be directly recovered from geological wireframes (as in: Machuca-Mory et al. 2015; and in this work); however, for these cases, the ranges of the local anisotropy must be inferred separately by some method to complete the LVA parameterization.

## CASE STUDY DATASET

The dataset studied herein is provided by Golden Star Resources from their Wassa gold deposit in Ghana. The Wassa gold mine is located approximately 40 kilometers northeast of the town of Tarkwa, Ghana. The mine lies within the southern Ashanti greenstone belt, and the gold mineralization is associated with quartz veining hosted in polydeformed greenstone rocks. The gold mineralization is structurally controlled, related to vein densities and sulfide content. The deposit has undergone multiple periods of deformation resulting in a complex folded structure along multiple fold axes (Fig. 1).

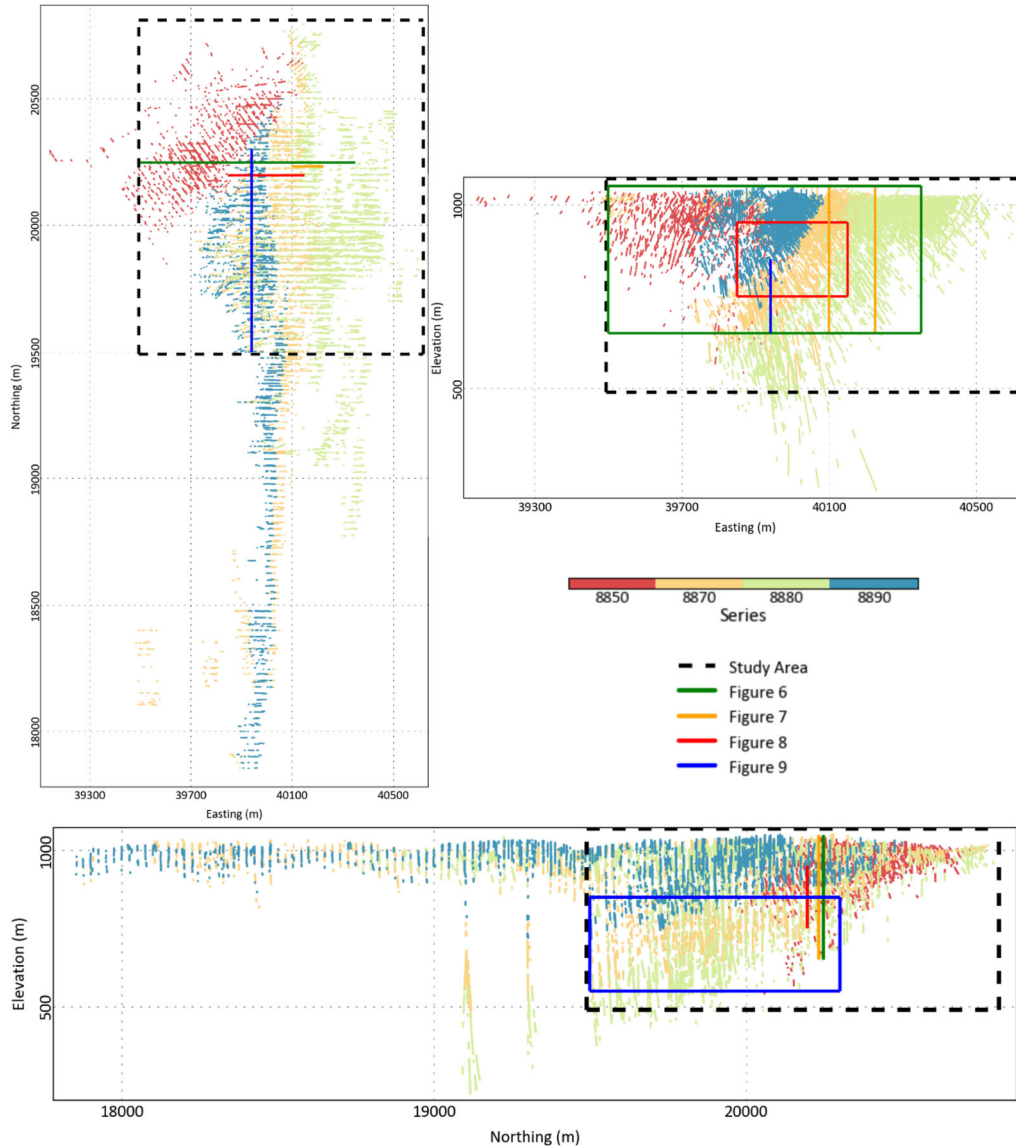


**Figure 1.** Plan view, E–W and N–S projected views through the domain, with samples coded by geological domain. The black dotted line represents the boundaries of the modeling area. The green, orange, red and blue boxes represent the boundaries of the slices plotted in Figures 6, 7, 8 and 9, respectively.

The goal of this work is to evaluate the different methods to: (1) model the required components of the LVA field; and (2) generate resource models with different LVA estimation algorithms. The gold mineralization is highly discontinuous at short ranges, and the geological interpretation is important for informing the local gold continuity. The dataset used for this study consists of 37,357 3-m gold composites from 1,824 drill holes, accompanied by a geological interpretation of the local continuities in the form of a geologic boundary wireframe. Drill

holes are mainly E–W oriented with a steep dip, intersecting an overall N–S striking and west-dipping folded mineralized structure (Fig. 1). The fold hinge is in the north portion of the project and plunges to the south-southwest at a moderate angle. For the purposes of this study, the domain is clipped to the northern region with dense sampling, outlined with the thick dotted line in Figure 1. Three-meter composite gold values range from detection limit to 56.97 g/t Au, with a mean value of 0.94 g/t Au; gold values are capped to 30 g/t. The samples are subset

into 4 estimation domains based on different structural zones of the folded strata bearing the mineralization. Variograms, cross-validation results and estimated grades are independently calculated in each estimation domain. The outcome of all modeling is evaluated by two criteria: (1) Models are visually inspected and evaluated based on continuity of local-grade estimates in structurally complex zones; and (2) the predictive performance of each algorithm is tested through a tenfold validation study by analyzing prediction errors from each LVA parameterization and estimation framework. Ordinary kriging in original units is used in this work. The estimation algorithms considered here include stationary kriging with an isotropic or anisotropic variogram model applied in stationary subdomains, and two LVA estimation frameworks: The first uses a location-dependent variogram (hereafter, LDV: Machuca-Mory and Deutsch 2013), and the second implements the space-deformation strategy (hereafter, SD: Boisvert and Deutsch 2011).

The geological boundary model defines the orientation and extents of mineralization for the targeted modeling domain; the boundaries and local orientations are shown in Figure 2. This interpretation is generated by geologists assessing the related samples and structural continuities observed based on local and regional experience at this project. Local orientations for the LVA field are extracted from this geological interpretation by processing the wireframe facets (Machuca-Mory et al. 2015). The resulting LVA orientations have no plunge component ( $ang3 = 0$ ); however, the strike and dip ( $ang1, ang2$ ) components vary smoothly throughout the domain and follow the model boundaries (Fig. 2).

### STATIONARY KRIGING PARAMETERS

The current domain is subset into 4 geological domains based on the structural continuities in different parts of the deposit. Ordinary kriging with a

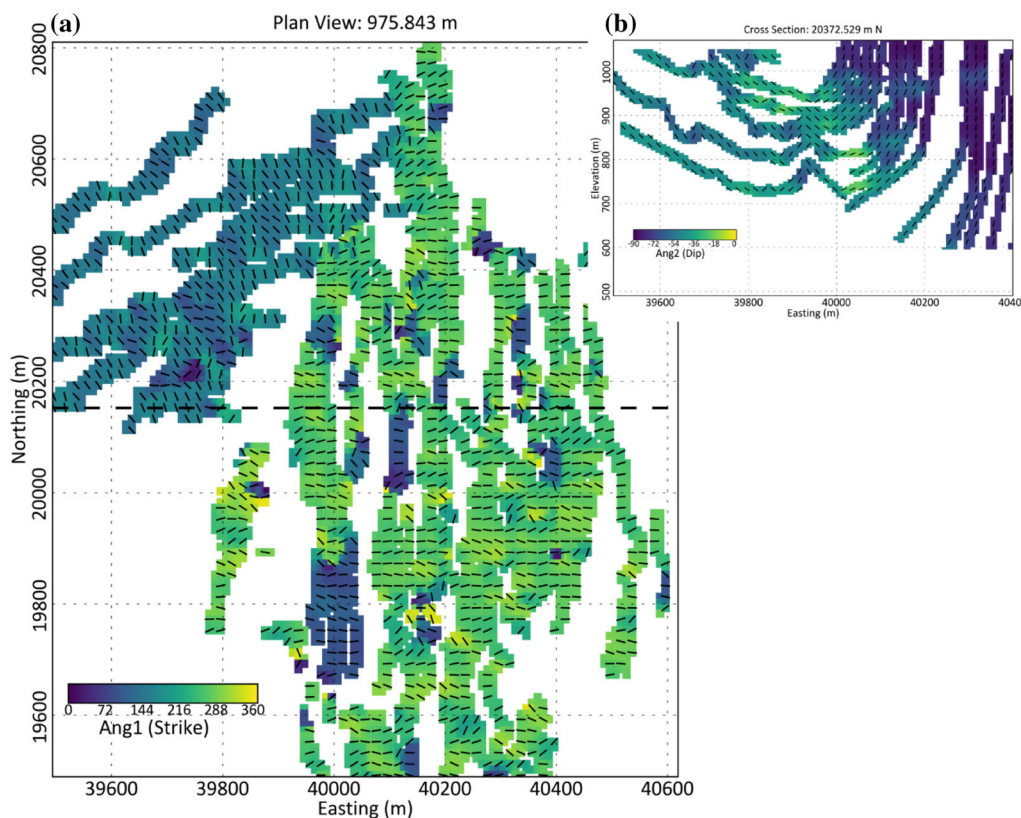


**Figure 2.** Selected slices of LVA orientations utilized for this study. (a) Plan view section showing the local strike orientation indicated with the heatmap and vector orientations. Location of the cross section in (b) shown with the dotted line. (b) XZ-slice showing complexity of the folded limbs.

stationary covariance function within each domain provides quasi-local anisotropy and represents the simplest method that can be used to account for local changes in anisotropy orientation.

In the presence of dense sampling, an isotropic variogram model can produce sufficiently local anisotropic estimates given the samples capture the local anisotropy of interest (Boisvert 2010). The experimental isotropic variogram is calculated for each estimation domain and modeled with a two-structure spherical variogram model (Fig. 3).

Inspection of the composite dataset and considering the modeled structural orientations indicated from the boundary model for each domain suggests that geometric anisotropy may better describe the grade continuity along the dipping model limbs. To test this hypothesis, the experimental variogram is calculated with the major axis oriented along the dipping limbs in each geological domain. Identifying three distinct directions of significantly different continuity for each sub domain was problematic, so a variogram model with

equal ranges in the rotated major and minor directions was chosen. The specific set of orientations for each domain are shown in Figure 4.

### NON-STATIONARY KRIGING PARAMETERS

The non-stationary estimation frameworks used here require local orientations and ranges defined at all locations in the estimation grid. This section highlights the methods used to estimate the local anisotropy ranges given the composite point data and local orientations extracted from the boundary model.

### Manual Interpretation

The range of anisotropy can vary with location in structurally complex domains with lognormally distributed grade variables. However, in certain

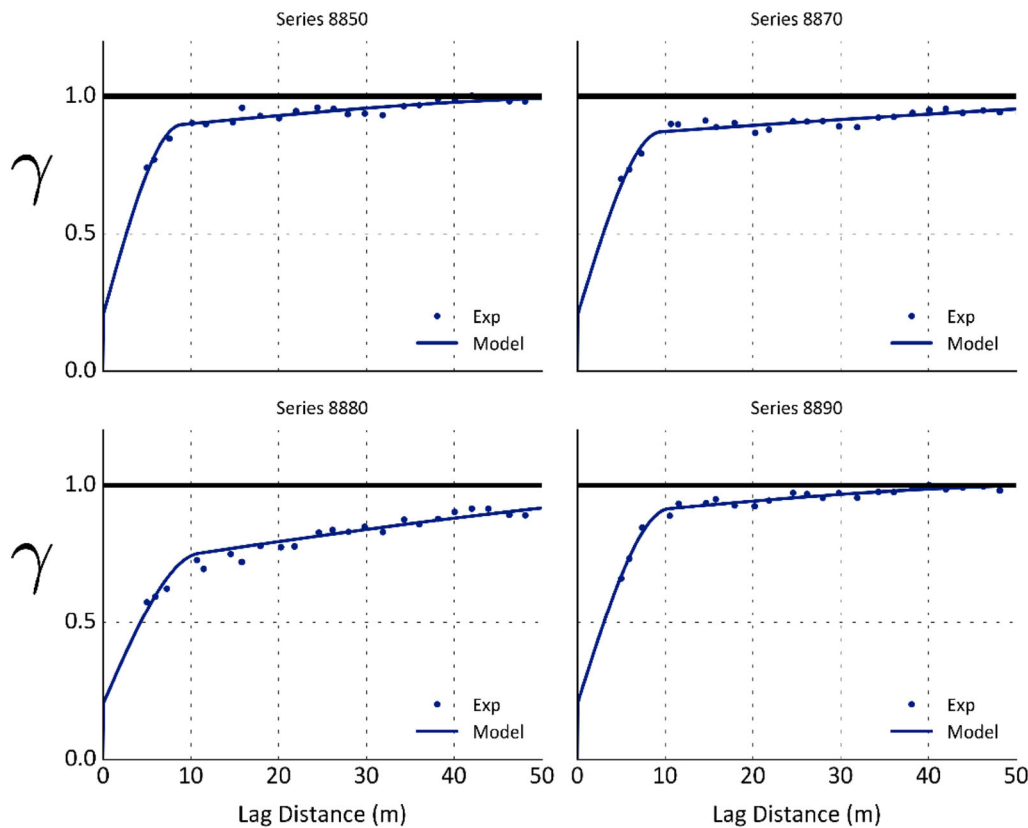
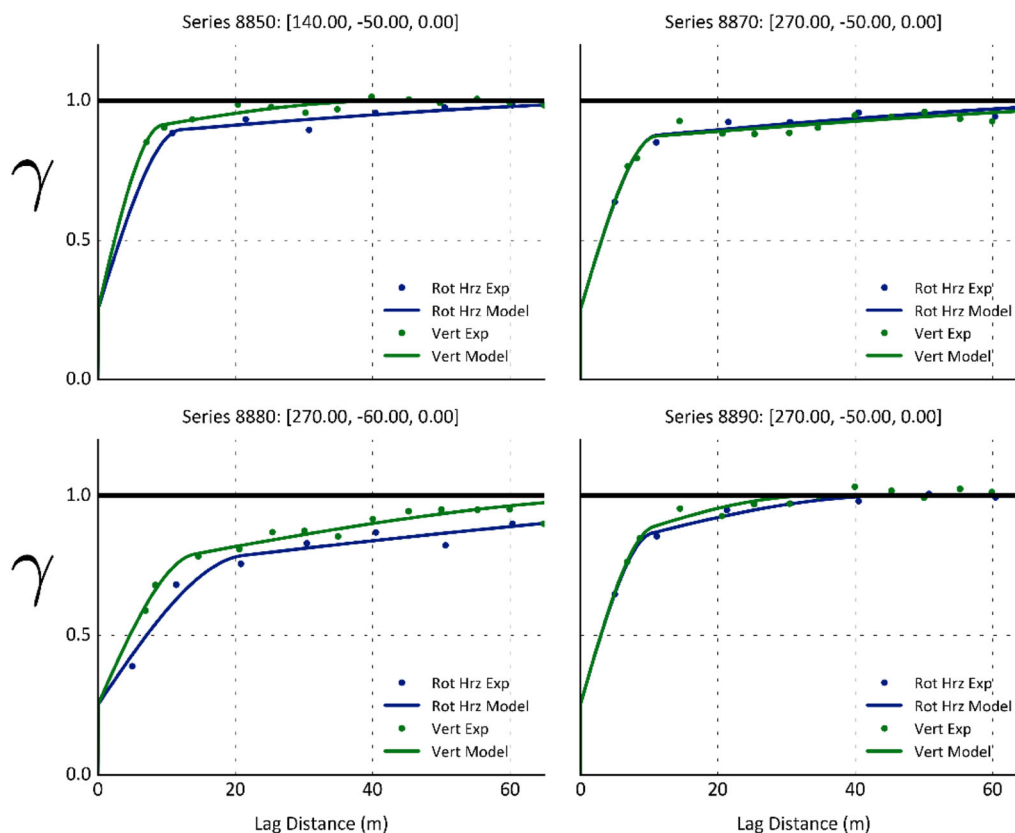


Figure 3. Experimental and model isotropic variograms for each geological series.



**Figure 4.** Experimental and modeled variogram for each geological series with listed [ang1, ang2, ang3] orientations for each domain. ‘Rot Hrzs’ refers to an isotropic variogram calculated in the rotated horizontal plane.

cases, a constant global range of anisotropy may be sufficient. Thus, the first set of ratios are based on the interpreted global continuity down dip and along strike of the dipping model limbs. The corresponding anisotropic ratios reflecting this interpretation of the grade continuity are:  $r_1 = 0.9$  and  $r_2 = 0.25$ .

**Cross-Validation**

Boisvert (2010) suggested to use cross-validation to choose sets of anisotropic ratios that better match the data. The starting set of ratios for cross-validation are  $r_1 = \{1.5, 0.8, 0.45, 0.2\}$  and  $r_2 = \{0.8, 0.35, 0.25, 0.05\}$ , generating 16 permuted sets of  $\{r_1, r_2\}$  tested for each domain and each estimation method. These anisotropic ratios reflect an interpretation primarily of down-dip continuity. Incorporating an  $r_1 > 1$  explores the hypothesis that the local primary direction of continuity is perpendicular to the local dip direction (ang1) in the rotated

horizontal plane. Since the samples are subset based on geological series, the ratios inferred in this manner are quasi-local since cross-validation is carried out independently in each subdomain. Cross-validation is performed independently for each of the LDV and SD estimation frameworks resulting in slightly different sets of best ratios for each estimation method.

**Distance-Weighted Local Variograms**

Local ranges of anisotropy can be extracted from the point dataset using the distance-weighted statistics from Machuca-Mory and Deutsch (2013). Recall that for complex 3D domains the local orientations are required to inform the direction for local variogram calculation. For this method, experimental distance-weighted variograms are constructed at anchor points located in different parts of the deposit and each geological domain

(Machuca-Mory et al. 2015). At each anchor location, the representative local orientation is calculated by distance-weighting the nearby LVA orientations taken from the geological boundary model. The local distance-weighted variograms are calculated and fitted with an appropriate model variogram where the range of anisotropy along each direction defines the required local ratios. Finally, the ratios are interpolated from the anchor locations to all required locations using global kriging with a large search and long-range variogram.

### Modified Distance-Weighted Local Variograms

A modification to calculated local variograms is proposed in this work, where pairs are categorized to either the major, minor or vertical variograms based on the orientations contained in the LVA field (Fig. 5; see “Appendix” for development of method). The idea is to use the orientation between data pairs compared against the average LVA orientation found along the lag vector between that pair. A conceptual example is shown in Figure 5. An average rotated coordinate system is calculated by considering the LVA orientations intersected along the

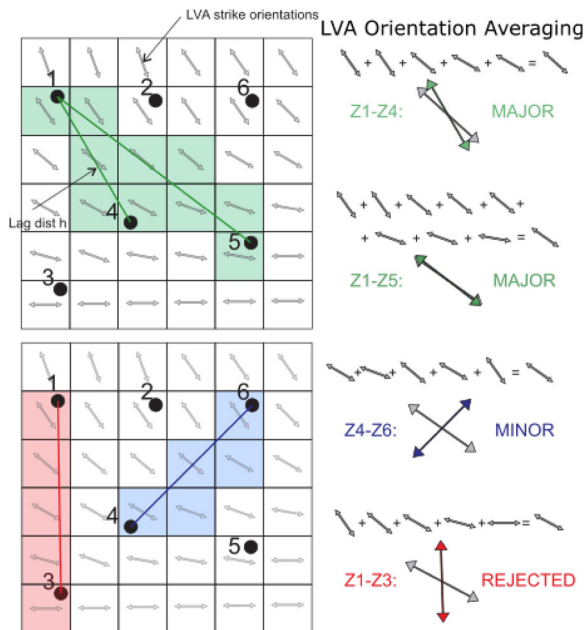


**Figure 5.** Conceptual LVA-pair matching methodology. Green cells indicate paths between pairs allocated to the major direction, blue cells indicate the path between a pair allocated to the minor direction, and red cells indicate path between a rejected pair.

lag vector between data locations. The angle between the lag vector and the principal axes of the average rotated coordinate system is calculated; if that angle is within a user-defined tolerance of one of the principal axes, the pair belongs to either the major, minor or vertical experimental variogram. Once LVA-pair (LVAP) classification is completed, a local experimental variogram is calculated and fitted using the same distance-weighting methodology as above. The benefit in considering this LVA-pairing method is that samples paired with one another depend on the LVA field rather than the location of the anchor points; in the latter case, the location chosen for each anchor fixes the variogram orientation and fixes the pairs used for each local variogram direction. Results from the two methods should be similar for locations where orientations are constant within local windows. Model ranges extracted from fitted variograms are smoothly interpolated to all unsampled locations, as above. This style of pairing is appropriate for LVA fields that vary smoothly, which should be the case; trends in anisotropy should not have abrupt changes, when such abrupt changes occur they should be considered by data domaining prior to the implementation of LVA techniques. For interested readers, details of the original and modified DWLV algorithm are given in “Appendix”.

### ESTIMATION RESULTS

Slices from all kriging runs are shown in Figures 6 and 7, and the results from the tenfold cross-validation for each estimation method and each set of LVA parameters are shown in Table 1. The main criteria used to evaluate each method are (1) visual inspection of the grade continuity along cross sections and (2) measures of the prediction performance for each estimation method including the correlation ( $\rho$ ) covariance ( $\Sigma$ ) and root-mean-squared-error (rmse) calculated between the estimated values and the true values. Grade estimates are considered better if the local continuity reflects the structural interpretation. The cross-validation results from all methods are similar. The non-stationary frameworks generate estimates with a higher covariance to the truth when compared to the stationary methods. Slices discussed in the following discussion refer to those from Figures 6 and 7.

Slices through estimates from the stationary techniques are shown in slices (a) and (b), respec-



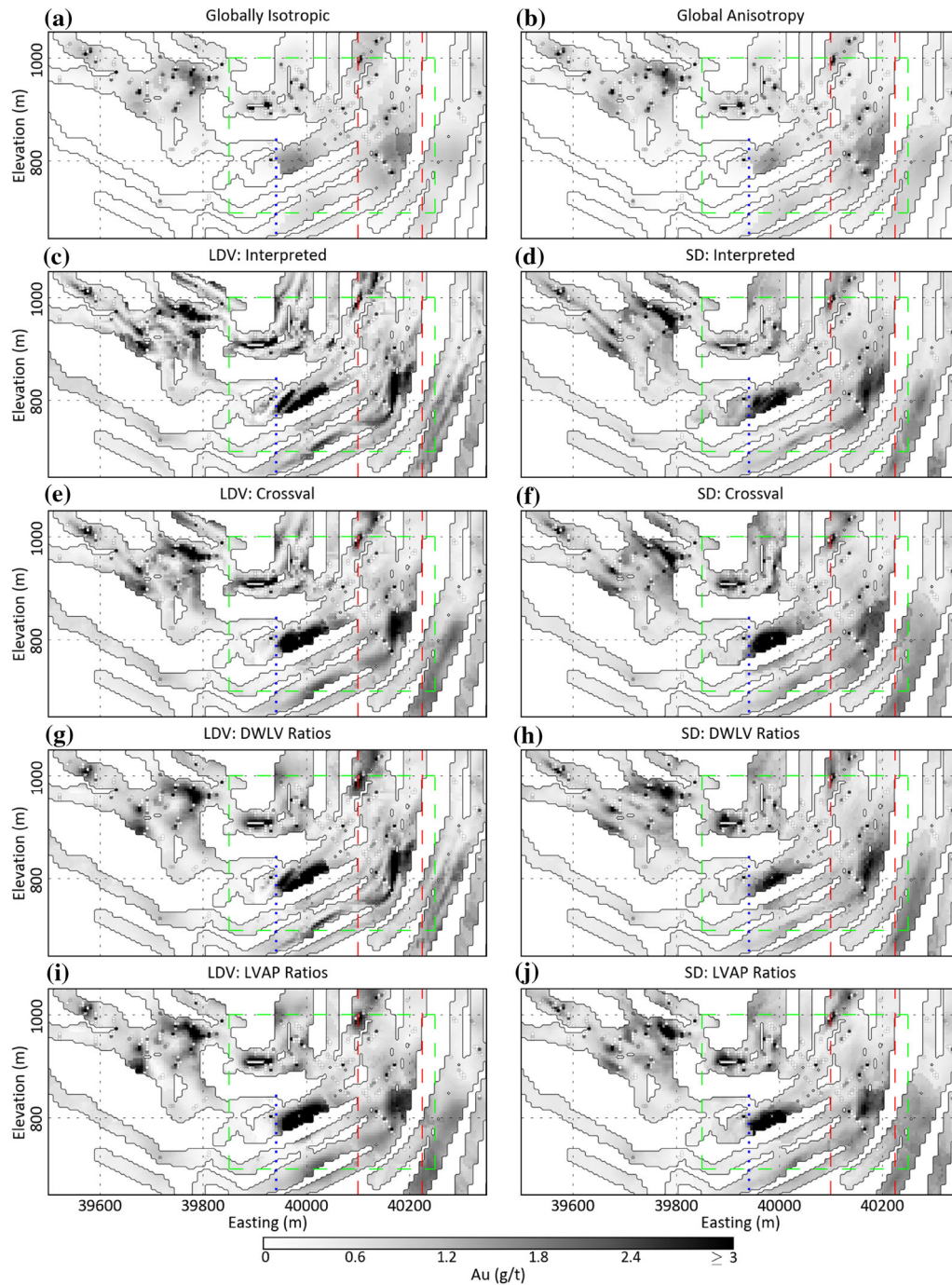


**Figure 6.** Clipped XZ slices through each model. Composite sample locations are shown. The red, green and blue dotted lines indicate the position of the zoomed slices shown in Figures 7, 8 and 9, respectively.

tively. Grade continuity in the isotropic case is limited even in densely sampled areas owing to the high short-range variability. Estimates generated using

domain-specific geometric anisotropy (with associated search parameters) improve upon the local continuity in the isotropic case since the estimates

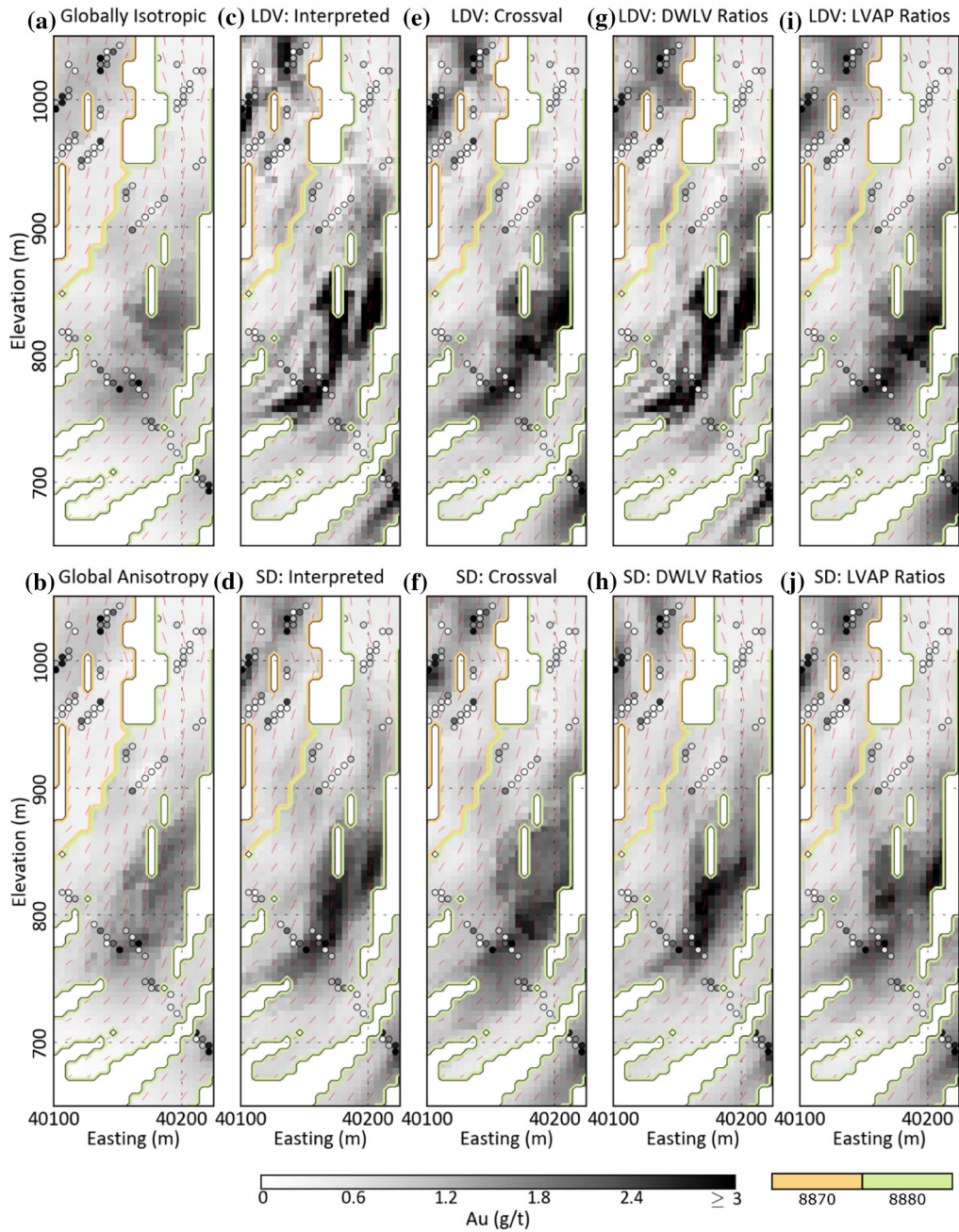


**Figure 7.** Zoomed slices through all models showing local differences. Model boundaries are shown with the bounding black line. Boundaries between subdomains shown in Figure 1 are shown as colored lines. LVA orientation vectors are drawn in red.

have improved down-dip continuity. Considering the similarity in variogram models for global isotropic and anisotropic cases, the observed differences can be attributed to the search parameters which were implemented to reflect the interpreted geometric

anisotropy by artificially shortening the vertical axis for all domains.

Non-stationary estimates generated using LDV kriging are shown in (c), (e), (g) and (i), and those from SD kriging are shown in (d), (f), (h), (j) in

Figure 6. The local continuity from non-stationary estimation over the global stationary methods is improved for both the LDV and SD kriging frame-

**Table 1.** Measures of cross-validation performance

Modeling parameters	$\rho$	cov	rmse
Stationary			
Global isotropic	0.272	0.276	1.727
Global anisotropy	0.278	0.294	1.724
LDV framework			
Interpreted ratios	0.258	0.355	1.762
Crossval ratios	0.256	0.347	1.761
DWLV ratios	0.239	0.361	1.790
LVAP ratios	0.258	0.376	1.769
SD framework			
Interpreted ratios	0.253	0.324	1.754
Crossval ratios	0.260	0.320	1.744
DWLV ratios	0.260	0.303	1.741
LVAP ratios	0.276	0.375	1.744

Correlation ( $\rho$ ), covariance (cov) and root-mean-squared-error (rmse) between the estimated values and the truth

**Table 2.** Final cross-validated anisotropic ratios for each subdomain

Domain	SD framework		LDV framework	
	$r_1$	$r_2$	$r_1$	$r_2$
8850	1.5	0.8	1.5	0.35
8870	0.8	0.8	0.8	0.35
8880	0.8	0.35	1.5	0.35
8890	0.45	0.35	1.5	0.25

The chosen ratios maximize the correlation between estimate and truth for each estimation framework

works and all sets of anisotropic ratios. The LDV and SD predictions have a small decrease in accuracy with lower  $\rho$  and higher rmse. This small increase in prediction error should be weighed against the improvement in local feature reproduction. Notably, predictions from both non-stationary frameworks have larger covariance to the truth.

The simplest anisotropic ratios generated by manual interpretation produced reasonable results with both estimation frameworks, although the strength of the anisotropy seems exaggerated with LDV kriging when compared to SD kriging. Anisotropic ratios generated by minimizing prediction errors using domain-specific cross-validation are tabulated in Table 2. The results from this method are improved since the ratios better match the local data and a different strength of anisotropy is possible at a smaller scale than the interpreted method. For example, in the top and bottom of Figure 7e and f, the strength of the local anisotropy between domains 8870 and 8880 varies. Interestingly, with both estimation frameworks, domain 8850 was found to have increased continuity along strike vs. down dip.

Finally, an LVA field generated by fitting local variograms to the point data results in better non-stationary estimates since the strength of the anisotropy reflects the local conditions. For example, in the top and bottom of Figure 7g and h, there is weak and strong anisotropy, respectively, which seems to fit each area better than the case of constant anisotropy or constant domain-specific anisotropy.

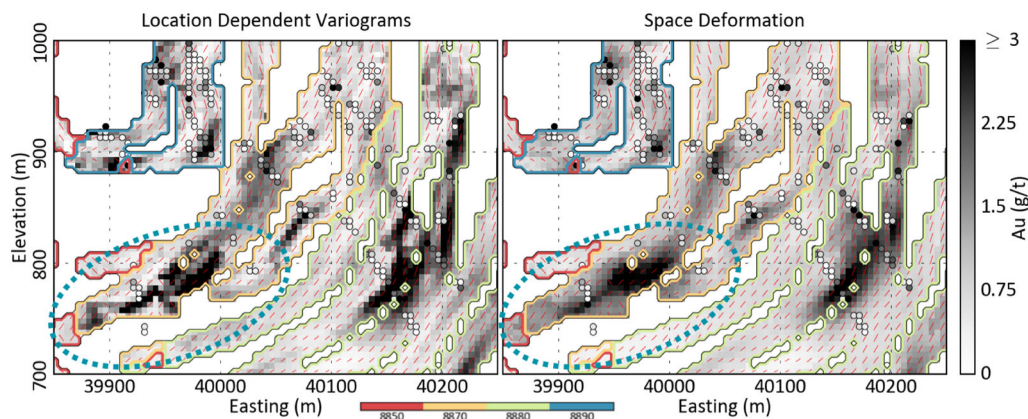


**Figure 8.** Zoomed XZ section through the east-central portion of the deposit. Boundaries between subdomains shown in Figure 1 are shown as colored lines. Vectors showing the local anisotropy orientation are shown in red. Dotted ellipse highlights areas where estimation frameworks differ.

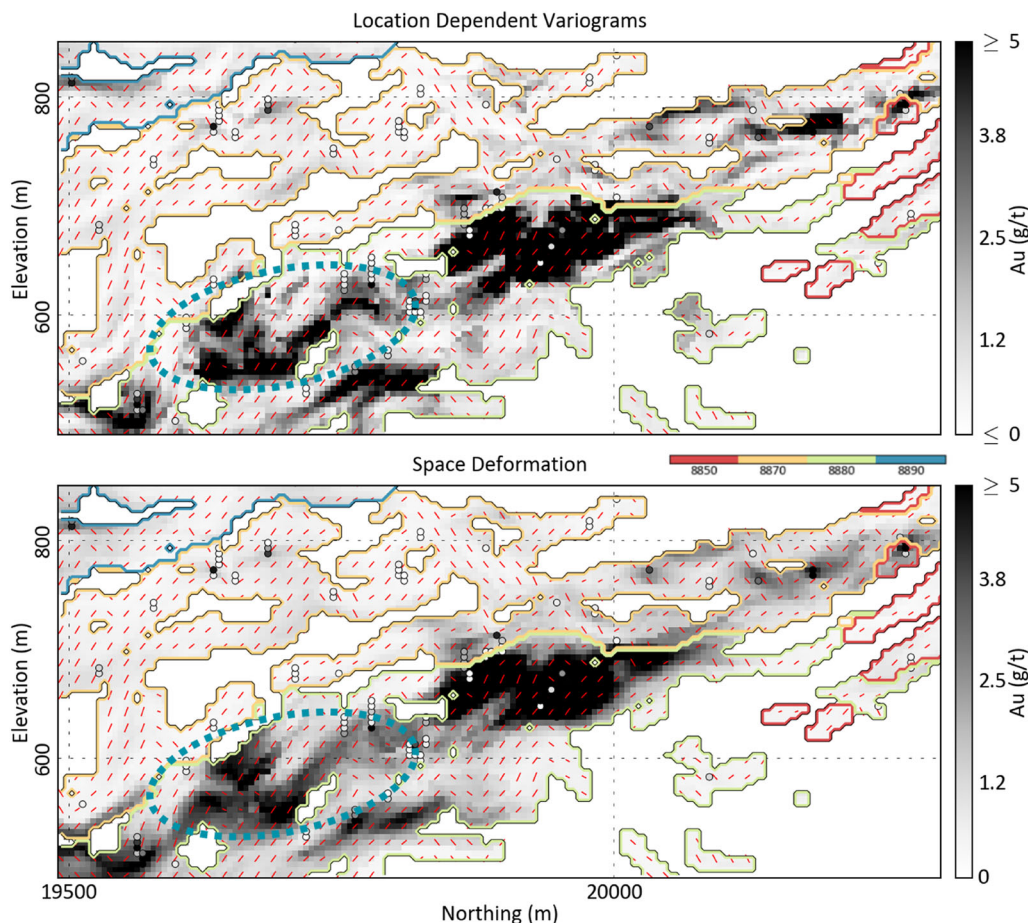


**Figure 9.** Zoomed YZ section through the central high-grade portion of the deposit. Boundaries between subdomains shown in Figure 1 are shown as colored lines. Vectors showing the local anisotropy orientation are shown in red. Dotted ellipse highlights areas where estimation frameworks differ.

## DISCUSSION

An important consideration for non-stationary estimation is the time required for each algorithm. In this work, the implementation of stationary kriging is from GSLIB (Deutsch and Journel 1998), the LDV implementation is from Machuca-Mory and Deutsch (2013) and the SD implementation is from Boisvert and Deutsch (2011). The modeling grid defined for the current domain has 6.9-M nodes, where 1.9-M is valid estimation locations (inside the geological boundary model). Stationary kriging requires 22.5 min, LDV kriging requires 42.5 min, and SD kriging requires 90.4 min to estimate at all blocks in the boundary model. The increase in time required reflects the increase in complexity between each method; the implementations considered here

could be optimized for CPU time, none of the codes consider parallelization, and all methods compared are very amenable to improved coding.

Overall, non-stationary estimation with space deformation generates estimates that are smoother than those generated from LDV kriging. For example, Figures 8 and 9 show slices through interesting locations in the models generated with LDV and SD kriging using the interpreted anisotropic ratios. An area showing the visible differences between LDV and SD kriging is circled with the blue ellipse. In areas where the local orientations are variable, estimates from SD kriging tend to vary smoothly between locations, whereas those generated from LDV kriging better match this local orientation variability. Consequently, the covariance between the estimate and truth from the LDV esti-

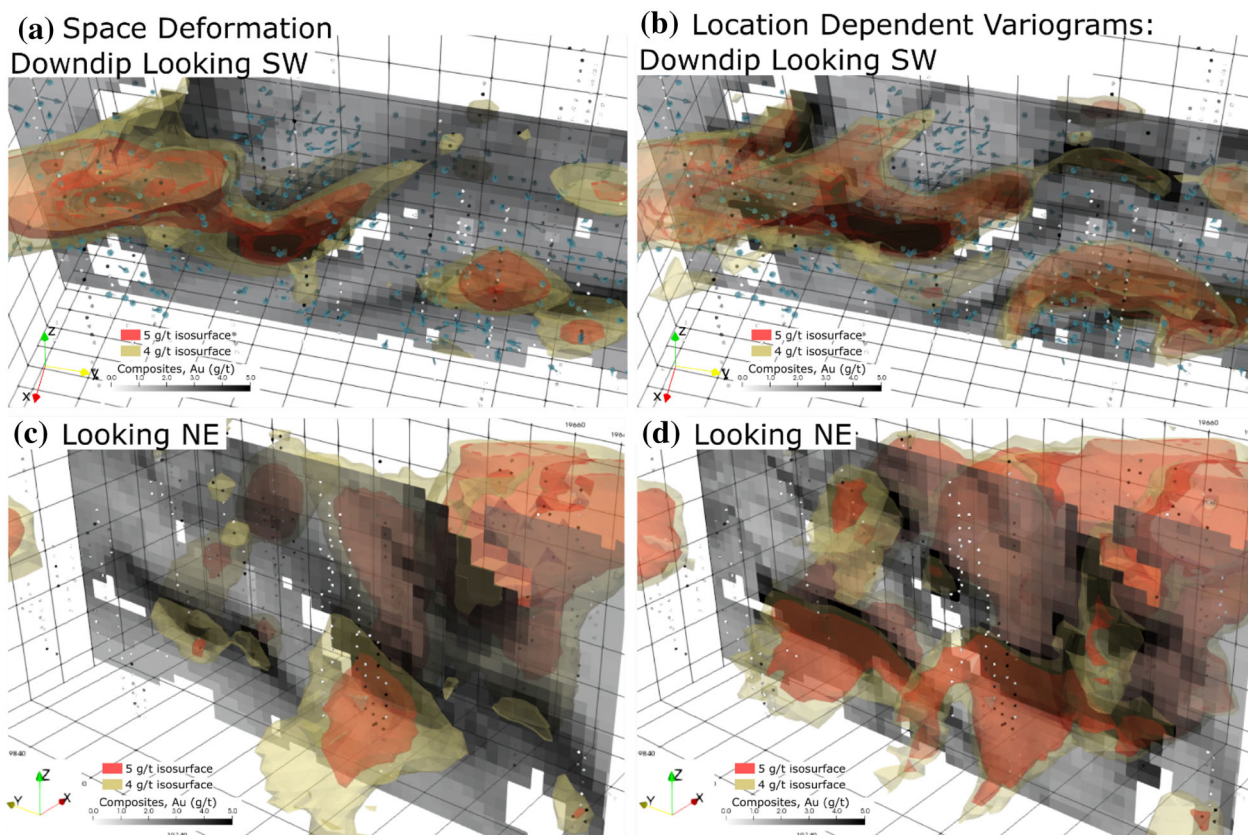


**Figure 10.** Rotated view of the circled ellipse in Figure 9, showing the off-section extension of the 4 g/t (yellow) and 5 g/t (red) isosurfaces of the grade model. Top: SW and down-dip oriented view with blue orientation vectors showing complex down-plunge folding patterns for the (a) SD and (b) LDV estimators. Bottom: view is roughly orthogonal to the dipping mineralization looking NE for the (c) SD, (d) LDV estimators, highlighting the smoothed nature of the SD grade model.

mator is higher, owing to the increased variance in the predictions (Table 1). The LDV estimator appears to have more sensitivity to locally variable orientations, whereas the SD estimator generates consistently smoother estimates with a pronounced diffuse contact between very high and low-grade zones. This diffusivity results in smooth transitions between zones of different grade value, which may be problematic given the short-range correlation of gold observed in the composite dataset.

A set of oblique views centered on the circled location in Figure 9 are shown in Figure 10 where the 4 and 5 g/t isosurfaces are plotted to show the off-section extension of the grade continuity for the two non-stationary estimation frameworks. Considering the down-dip view (Fig. 10a and b), both frameworks generate the expected curvilinear features indicated from the LVA field in this location. The LDV estimation method generates better down-

plunging folded structures considering this view. Figure 10c and d shows the down-plunge extent of the high-grade zone. The difference in model smoothing is apparent; although the locally oriented zones are consistent in the non-stationary methodology, there is additional distance between the 4 and 5 g/t shell for SD kriging. Boisvert (2010) notes that the dimensionality reduction required to ensure positive definite kriging matrices introduces some errors in distance calculations in the high-dimensional spaces, and the effect is especially pronounced at the short range. Given the short-range nature of grade continuity in this domain, this is a significant limitation in applying this space-deformation method here.

Another interesting difference between the frameworks is the search implementation and how the local samples are related to one another within the constraints of the boundary model. The imple-

mentation of SD kriging from Boisvert and Deutsch (2011) uses a weighted graph to parameterize connectivity between locations and calculate nonlinear distances. Although locations in adjacent limbs may be close based on their Euclidean position, the connected graph and deformed space ensures they are very far away since the shortest path must follow connected estimation locations within the boundary model. Reproducing the isolation of data within each model limb with the LDV methodology is difficult. Since data from adjacent model limbs may be easily found in a locally reoriented search with LDV kriging, the only way to ensure consistent sets of data are used within each model limb is to isolate and model data from each limb independently. In this respect, the LVA-pair matching algorithm improves the data selection for the local variograms by matching data pairs that are effectively connected based on the LVA field.

## CONCLUSIONS

Parameterizing the LVA field is the main consideration for implementing LVA for grade estimation. Extracting local orientations from an external source is ideal since information is added that cannot be derived from the point dataset. Several methods can be used to parameterize both the orientations and magnitudes of anisotropy that complete an LVA specification, depending on the complexity of the local orientations, the nature of the grade variability and the amount of professional time allotted for non-stationary inference. Given a set of local anisotropic orientations, as a first pass, an interpreted local ratio is sufficient. Domain-specific cross-validation generates improved results with some additional scripting efforts. Fitting local variograms is the ideal method to parameterize the local ratios; however, this is the most complex to implement. Although the extension for local experimental variograms calculated from pairs generated using the average LVA field is interesting, the tight constraints of the bounding model in the current domain limited the utility of this method for this project. The likely issue stems from the domain boundaries and the current implementation, which follows a straight-line path and considers two points to be unconnected if a boundary is encountered in this path. Additional work is required to account for complex domain boundaries and this LVA-pairing methodology.

This study also showed that the choice of non-stationary estimation framework does impact the final estimates, both in terms of statistical reproduction and local non-stationary feature reproduction. The smoothing effect of the SD framework considered herein was pronounced, though, both non-stationary estimation frameworks generated estimates with better local feature reproduction that considering stationary methods. The overall poor statistical performance for this domain can be attributed to the high nugget effect. Given the improvement in local feature reproduction, the minor increase in prediction errors is deemed acceptable. Second-order non-stationary estimation methods are effective in capturing curvilinear features in structurally complex domains. How the LVA is parameterized and used to build conditional distributions at the unsampled locations within the non-stationary interpretation affects the resulting grade estimates.

## ACKNOWLEDGMENTS

We would like to thank the member companies of the Center for Computational Geostatistics for their support of this research and Golden Star Resources Ltd. for providing data from its Wassa gold project for this study.

## APPENDIX

### Details of the DWLV Parameter Inference Framework

To extract the LVA ratio's from the DWLV's, first a set of anchors are defined by partitioning the domain based on the data density or by considering regions of quasi-constant orientations using an algorithm such as K-means clustering. An orientation for local variogram calculation at each anchor location must be inferred. Machuca-Mory and Deutsch (2013) note that in 2D cases the local orientations can be inferred from the data, but in 3D additional information is required.

Once the anchors and local orientations for each anchor are defined, an experimental variogram is constructed by weighting the square difference of

the data pairs by the geometric average of the weights assigned to each sample:

$$wt_{c_{ij}} = \sqrt{wt_{c_i} \cdot wt_{c_j}}$$

where  $wt_{c_i}$  and  $wt_{c_j}$  are the weights based on the distance between the samples locations  $u_i$  and  $u_j$  to the current anchor  $c$ . These weights can be inverse-distance weights (IDW) or weights from a Gaussian kernel centered on  $c$ . It should be noted that weighting from Gaussian kernels provides a more continuous and stable weighting of data between anchor locations (Machuca-Mory and Deutsch 2013). The weighted variogram for each anchor  $c$  and for each lag  $h$  is calculated as (Machuca-Mory and Deutsch 2013):

$$\gamma(h; c) = \frac{1}{2 \sum_{i=1}^n \sum_{j=1}^n wt_{c_{ij}}} \sum_{i=1}^n \sum_{j=1}^n wt_{c_{ij}} (z(u_i) - z(u_j))^2$$

All distances refer to the Euclidean distance, and  $|u_i - u_j| \cong |h|$ . The constructed experimental variograms can be fit manually or semiautomatically

to determine the local range of anisotropy (and ratios) at each anchor location. The final fitted ratios can then be interpolated smoothly throughout the domain using global kriging with a long variogram range or IDW interpolation.

**Modified LVA-Pair Matching Algorithm**

A modified version of DWLV is proposed where instead of determining a representative local orientation for each anchor location, each data pair is individually classified as along major, minor or vertical directions based on the pair orientation and the LVA orientations found along the lag vector. To obtain the average orientation along the lag vector in 2D vector components may be averaged if the axial nature of the data is accounted for. However, in 3D where the local orientations include a plunge, quaternions are used to determine the average rotated coordinate system (Markley et al. 2007). For every intersected cell along the straight-line path,

$$M = \sum_{i=1}^{ni} q_i q_i^T$$

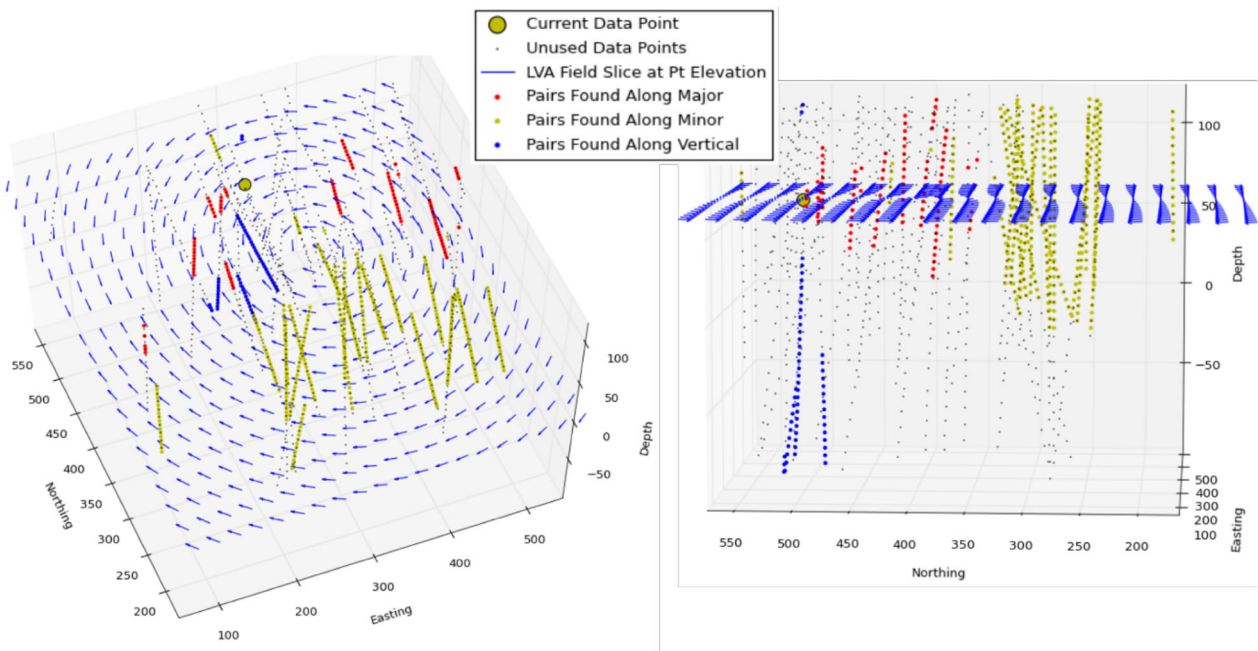


**Figure 11.** LVA-pair classification for all pairs matched to a single data point, shown in the large yellow circle. Red points are along the major direction, yellow points along the minor direction, and blue points are along the vertical direction.

the rotation angles strike  $\alpha$ , dip  $\beta$  and plunge  $\phi$  (ang1, ang2, ang3 from GSLIB conventions) are converted to a quaternion using (Lillah and Boisvert 2015):

$$q(\alpha, \beta, \phi) = \begin{bmatrix} \cos\left(\frac{\phi}{2}\right) \cos\left(\frac{\beta}{2}\right) \cos\left(\frac{\alpha}{2}\right) - \sin\left(\frac{\phi}{2}\right) \sin\left(\frac{\beta}{2}\right) \sin\left(\frac{\alpha}{2}\right) \\ \cos\left(\frac{\phi}{2}\right) \sin\left(\frac{\beta}{2}\right) \cos\left(\frac{\alpha}{2}\right) - \sin\left(\frac{\phi}{2}\right) \cos\left(\frac{\beta}{2}\right) \sin\left(\frac{\alpha}{2}\right) \\ \cos\left(\frac{\phi}{2}\right) \sin\left(\frac{\beta}{2}\right) \sin\left(\frac{\alpha}{2}\right) - \sin\left(\frac{\phi}{2}\right) \cos\left(\frac{\beta}{2}\right) \cos\left(\frac{\alpha}{2}\right) \\ \cos\left(\frac{\phi}{2}\right) \cos\left(\frac{\beta}{2}\right) \sin\left(\frac{\alpha}{2}\right) - \sin\left(\frac{\phi}{2}\right) \sin\left(\frac{\beta}{2}\right) \cos\left(\frac{\alpha}{2}\right) \end{bmatrix}$$

and the matrix  $M$  is accumulated using the outer product, for all intersected cells,  $ni$ , between each data pair (Markley et al. 2007):

$$M = \sum_{i=1}^{ni} q_i q_i^T$$

Finally, the quaternion representing the average rotated coordinate system is the eigenvector corresponding to the largest eigenvalue from Eigen decomposition of the matrix  $M$  (Markley et al. 2007). The set of strike, dip and plunge is recovered using (Lillah and Boisvert 2015):

$$\begin{bmatrix} \alpha \\ \beta \\ \phi \end{bmatrix} = \begin{bmatrix} \arctan 2(-2q_1q_3 + 2q_0q_2, q_3^2 - q_2^2 - q_1^2 + q_0^2) \\ \arcsin(-2q_2q_3 + 2q_1q_0) \\ \arctan 2(-2q_1q_2 + 2q_0q_3, q_2^2 - q_3^2 - q_0^2 + q_1^2) \end{bmatrix}$$

where  $q_1, q_2, q_3$  and  $q_4$  are the respective components of the average quaternion.

Examples of pair matching using the LVA field are shown for a simple domain in Figures 11 and 12. The LVA interpretation for this domain is circular with no dip component. Figure 11 shows a slice of the LVA field for a z-value centered at the large yellow point. All pairs that utilize this point are plotted and colored according to their coding as either along the major, minor or vertical directions from this methodology. Pairs in each direction are logically arranged in this LVA field; major pairs are oriented outwards along the direction of largest continuity indicated from the LVA vectors, minor pairs are oriented roughly 90 degrees to the major orientation, and the vertical pairs are above and below the current pair (Fig. 11). Figure 12 shows the straight-line path between a single data pair. LVA intersected in the cells each end of the lag vector is drawn, and the average rotated coordinate system is calculated from the intersected cells. The pair in Figure 12 is coded to the major variogram because the orientation of the lag vector for this pair is

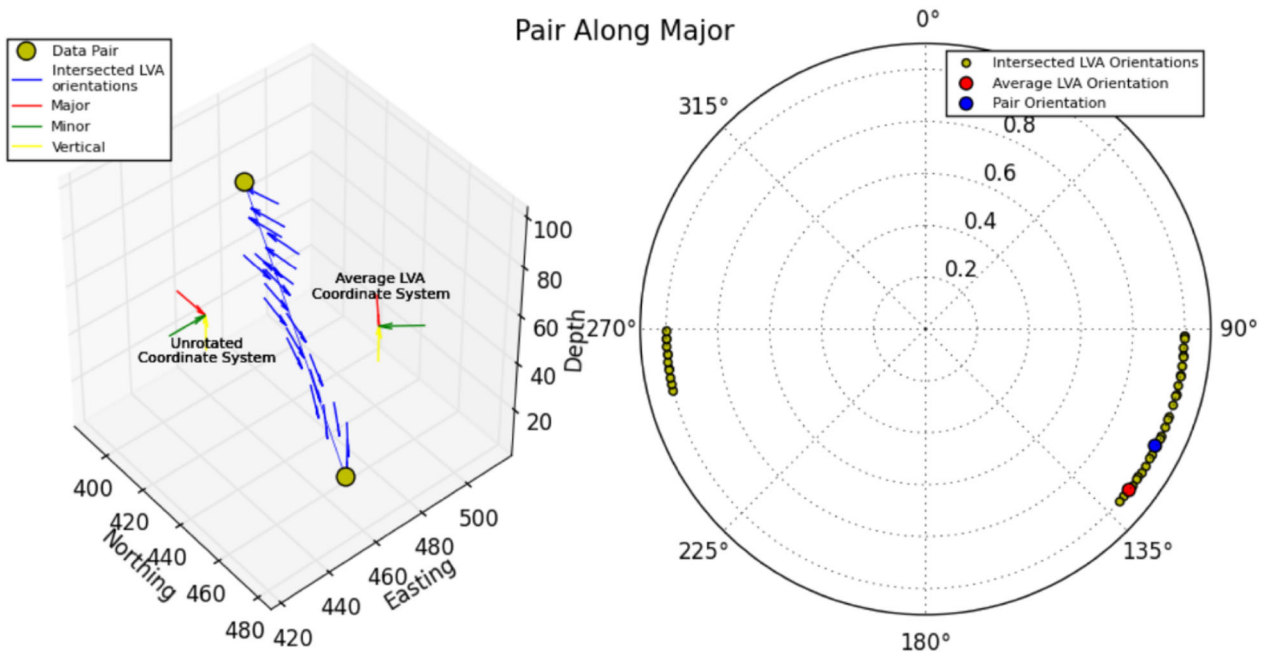


**Figure 12.** For a single data pair, the average strike vectors are shown on the left, and the average rotated coordinate system along with the pair orientation are shown to the right. This pair is classified as along the major direction.



coincident with the major axis of the average rotated coordinate system.

## REFERENCES

- Boisvert, J. B. (2010). *Geostatistics with locally varying anisotropy*. PhD Thesis, University of Alberta.
- Boisvert, J. B., & Deutsch, C. V. (2011). Programs for kriging and sequential Gaussian simulation with locally varying anisotropy using non-Euclidean distances. *Computers & Geosciences*, 37(4), 495–510.
- Deutsch, C. V., & Journel, A. G. (1998). *GSLIB: Geostatistical software library and user's guide* (2nd ed.). New York: Oxford University Press.
- Fouedjio, F. (2015). Space deformation non-stationary geostatistical approach for prediction of geological objects: Case study at El Teniente Mine (Chile). *Natural Resources Research*, 25(3), 283–296.
- Fouedjio, F. (2016). Second-order non-stationary modeling approaches for univariate geostatistical data. *Stochastic Environmental Research and Risk Assessment*, pp. 1–20.
- Fouedjio, F., Desassis, N., & Rivoirard, J. (2016). A generalized convolution model and estimation for non-stationary random functions. *Spatial Statistics*, 16, 35–52.
- Fouedjio, F., Desassis, N., & Romary, T. (2015). Estimation of space deformation model for non-stationary random functions. *Spatial Statistics*, 13, 45–61.
- Fouedjio, F., & Seguret, S. (2016). Predictive geological mapping using closed-form non-stationary covariance functions with locally varying anisotropy: Case study at El Teniente Mine (Chile). *Natural Resources Research*, 25(4), 431–443.
- Lillah, M., & Boisvert, J. B. (2015). Inference of locally varying anisotropy fields from diverse data sources. *Computers & Geosciences*, 82, 170–182.
- Machuca-Mory, D. F., & Deutsch, C. V. (2013). Non-stationary geostatistical modeling based on distance weighted statistics and distributions. *Mathematical Geosciences*, 45(1), 31–48.
- Machuca-Mory, D. F., Rees, H., & Leuangthong, O. (2015). Grade modelling with local anisotropy angles: A practical point of view. In *37th Application of computers and operations research in the mineral industry (APCOM 2015)*.
- Markley, F. L., Cheng, Y., & Crassidis, J. L. (2007). Averaging quaternions. *Journal of Guidance, Control and Dynamics*, 30(4), 1193–1197.
- Martin, R., & Boisvert, J. B. (2017). Iterative refinement of implicit boundary models for improved geological feature reproduction. *Computers and Geosciences*, 109, 1–15. <http://doi.org/10.1016/j.cageo.2017.07.003>.
- McBratney, S. B., & Minasny, B. (2013). Spacebender. *Spatial Statistics*, 4, 57–67.
- Rossi, M. E., & Deutsch, C. V. (2014). *Mineral resource estimation* (1st ed., Vol. 1). Springer Science.
- Sullivan, J., Satchwell, S., & Ferrax, G. (2007). Grade estimation in the presence of trends—The adaptive search approach applied to the Andina Copper Deposit, Chile. In *Proceedings of the 33rd international symposium on the application of computers and operations research in the mineral industry. GECAMIN Ltd. 2007* (pp. 135–143).
- te Stroet, C. B. M., & Snepvangers, J. J. J. C. (2005). Mapping curvilinear structures with local anisotropy kriging. *Mathematical Geology*, 37(6), 635–649.
- Xu, W. (1996). Conditional curvilinear stochastic simulation using pixel-based algorithms. *Mathematical Geology*, 28(7), 937–949.